



On Integration of Vibration Suppression and Energy Harvesting Through Piezoelectric Shunting With Negative Capacitance

Ting Wang , Graduate Student Member, IEEE, Joshua Dupont, Student Member, IEEE, and Jiong Tang, Member, IEEE

Abstract—While negative capacitance (NC) element has the potential of increasing the apparent electro-mechanical coupling in various piezoelectric applications, it generally requires a power supply which may negate its benefit. Indeed, there has been no systematic analysis of NC power consumption in piezoelectric circuitry. In this article, we investigate the combinatorial effect of NC circuit on an integrated design of passive vibration suppression and energy harvesting with LC resonant shunt. We first conduct a power consumption analysis of a representative NC circuit and analyze its influence on piezoelectric energy harvesting. We then explore the tradeoff between vibration suppression through LC shunt with NC element and the net power generation of the energy harvester. It is identified that there exists a range of NC values within which the vibration suppression performance is enhanced while the net power generation remains to be positive. This effectively yields a self-sustainable vibration suppression enhancement scheme with an NC element. Correlated numerical and experimental studies confirm this new finding.

Index Terms—Energy harvesting, LC resonant shunt, negative capacitance (NC), net power, piezoelectric transducer, vibration suppression.

I. INTRODUCTION

BECAUSE of their two-way electro-mechanical coupling effect, piezoelectric transducers have been widely used for control, sensing, and energy harvesting applications [1]. For example, they have been employed in various passive control schemes to facilitate vibration suppression. Typically, a piezoelectric transducer is bonded to or embedded in a host mechanical structure to convert vibration energy into electrical

Manuscript received 7 April 2022; revised 7 November 2022; accepted 3 February 2023. Date of publication 9 March 2023; date of current version 17 October 2023. This work was supported in part by the NSF under Grant CMMI–1825324 and in part by the DOT Transportation Infrastructure Durability Center at the University of Maine under Grant 69A3551847101. Recommended by Technical Editor S. Laghrouche. (Corresponding author: Jiong Tang.)

The authors are with the Department of Mechanical Engineering, University of Connecticut, Storrs, CT 06269 USA (e-mail: ting.2.wang@uconn.edu; joshua.dupont@uconn.edu; jtang@engr.uconn.edu).

Color versions of one or more figures in this article are available at https://doi.org/10.1109/TMECH.2023.3249635.

Digital Object Identifier 10.1109/TMECH.2023.3249635

energy [2]. Circuitry elements are then employed to form shunt circuits to absorb and/or dissipate the electrical energy [3], [4]. This concept is versatile, can be effective in various frequency ranges, and requires none or minimal ancillary supports in terms of controller and power supply. A classical design was attributed to Hagood and Von Flotow who suggested connecting an inductor (L) and a resistor (R) in series with the piezoelectric transducer [5]. This leads to an *RLC* shunt where the piezoelectric transducer behaves electrically like a capacitor (C), which is analogous to a tuned mass damper. The selection/tuning of the RL elements can be decided by minimizing the transfer function between the mechanical displacement and external disturbance, which is again analogous to tuned mass damper optimization [6]. Since then, a variety of efforts have been attempted, aiming at enhancing the vibration suppression performance. Examples of advancements include tuning criterion improvement [7], nonlinear circuit design [8], tunable circuit [9], multimode vibration suppression [10], switching circuit [11], etc.

An important parameter that affects the performance of a passive piezoelectric vibration suppression device is its coefficient of electro-mechanical coupling between the mechanical host structure and the shunt circuit. This parameter is primarily decided by the electro-mechanical coupling constant of the piezoelectric transducer which is a material property as well as by other factors such as transducer size and location and the vibration mode of interest, etc. Adopting piezoelectric transducers with higher electro-mechanical coupling constant can lead to better performance [12]. The electro-mechanical coupling coefficient at the device level is also related to the capacitance of the piezoelectric transducer. Indeed, during vibration, the piezoelectric capacitance traps a considerable portion of system energy which cannot be released into the shunt circuit for storage and dissipation. To overcome this, there has been a series of research employing a negative capacitance (NC) element to offset the inherent piezoelectric capacitance [13], [14], thereby increasing the apparent electro-mechanical coupling coefficient [15], [16], [17], [18], [19]. The NC element is usually realized through the usage of negative impedance converter (NIC), an op-amp-based circuit with power supply [20], [21]. An intriguing factor in this case is that the originally passive vibration suppression device then requires a power supply, losing the passive nature [22]. It is worth mentioning that, although not investigated in this

research, NC circuit has seen usage in the design of piezoelectric metamaterials for wave guiding and vibration suppression [23], [24], [25], [26], [27]. Similarly, the related devices may lose the passive nature.

Meanwhile, piezoelectric transducers have been widely investigated for energy harvesting research, i.e., turning ambient vibration energy into electrical energy to either directly power devices or recharge batteries connected to devices [28], [29], [30]. In many ways similar to vibration suppression research, the energy harvesting research has seen various explorations in both mechanical design [31] and shunt circuit synthesis to improve performance through, for example, resonance generation [32], impedance matching [33], multimode [34], wideband harvesting [35], and nonlinearity introduction [36] for the amplification of transducer deformation, etc. Fundamentally, these designs aim at tailoring the dynamics of the energy harvesting devices to amplify the power output.

Having a higher electro-mechanical coupling coefficient can certainly yield better performance of energy harvesting. Some recent studies looked into integrating NC elements into piezo-electric energy harvesting [37]. However, there does not seem to be a clear conclusion on how this integration will improve the net power generation, in part owing to the complexity involved in the power analysis of the NC circuit. It is worth noting that a systematic assessment of the NC circuit in terms of power consumption has yet to be fully established.

Consider the performance enhancement of passive piezoelectric vibration suppression with NC element. Also consider piezoelectric energy harvesting and its potential enhancement with NC element. It is actually tempting to integrate these two schemes together to form a concurrent design sharing the same circuitry configuration and examine if it is possible to construct a device that possesses enhanced vibration suppression performance due to NC, and at the same time remains to be passive without the need of constant, external power supply owing to the energy harvesting capability. That is, we want to explore if it is possible to take advantage of piezoelectric energy harvesting, through the same transducer and circuitry, to synthesize a selfsustainable NC. In a practical situation, an intermediate energy storage element such as a rechargeable battery may still be used from which the NC element can constantly draw power and to which the energy harvester can constantly supply power. This will eliminate the need for battery replacement or external power source to facilitate enhanced vibration suppression. Without loss of generality, in this research, we adopt the classical RL shunt for both vibration suppression and energy harvesting and investigate systematically how the integration of NC element influences vibration reduction and generation of net power (i.e., the difference between power generated by the integrated device and the power consumed by the NC circuit).

The rest of this article is organized as follows. In Section II, we briefly outline the system equations and the basic tuning criteria for optimal vibration suppression, where the benefit of NC to the vibration suppression aspect is illustrated. Section III focuses on analyzing in detail the power consumption of a representative NC element built upon op-amp circuit. This analysis can be applied to various applications involving NC circuit. In

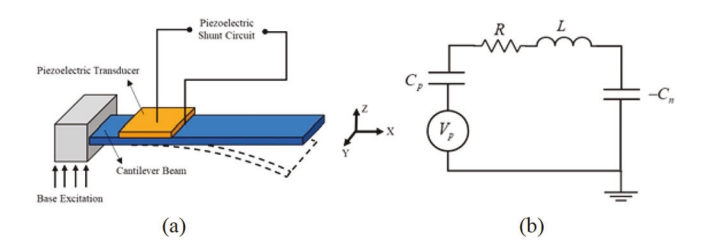


Fig. 1. (a) Schematic of a piezoelectric shunt circuit system. (b) Equivalent circuit of the transducer with shunt.

TABLE I
PARAMETERS OF CANTILEVER BEAM

Parameter	Value	Unit
Length	0.210	m
Width	0.030	m
Thickness	0.00317	m
Density	2842	kg/m^3
Young's modulus	69	GPa
Damping ratio	0.0105	_

Section IV, we present the method for net power analysis of the energy harvesting aspect, and we elucidate the possibility of synthesizing a self-sustainable system with enhanced vibration suppression through NC integration. Section V provides experimental confirmation of the research components. Finally, Section VI concludes this article.

II. SYSTEM EQUATIONS AND VIBRATION SUPPRESSION TUNING

A. System Equations and Transfer Functions

We consider a piezoelectric shunt integrated with a host structure, as shown in Fig. 1(a), where a unimorph piezoelectric transducer is bonded onto a cantilever beam and connected in series with an inductor L and a resistor R. Fig. 1(b) illustrates the equivalent circuit of the piezoelectric transducer consisting of a voltage source and an inherent capacitance C_p . As shown in literature [2], [3], [38], and [39], a simplified form of the equations of motion of this system can be derived as

$$m\ddot{q}+g\dot{q}+kq+k_1Q=F$$

$$L\ddot{Q}+R\dot{Q}+k_2Q+k_1q=0 \tag{1a,b}$$

where q is the structural displacement and Q is the charge flow in the shunt circuit. m, g, and k are, respectively, the equivalent mass, damping, and stiffness coefficients corresponding to the mode of interest. L, R, and k_2 are the inductance, resistance, and the reciprocal of the inherent piezoelectric capacitance. k_1 is the electro-mechanical coupling constant of the piezoelectric transducer. While a variety of modeling approaches exist, here we apply the combination of Hamilton's principle and assumed mode method [2]. Without loss of generality, we use the first mode of the cantilever beam as the basis for discretization. The parameters involved in ((1a) and (1b) can be computed based on results shown in literature [2], [38]. Tables I and

TABLE II
PARAMETERS OF PIEZOELECTRIC TRANSDUCER

Value	Unit
0.011	m
0.0701	m
0.030	m
0.0026	m
7983	kg/m ³
63	GPa
11.41	nF
7.0889e+07	Nm^2/C^2
2.5483e+08	N/C
	0.011 0.0701 0.030 0.0026 7983 63 11.41 7.0889e+07

II list the geometry and material properties of the beam and the piezoelectric transducer. The material properties have been slightly updated based on the vendor data with the aim of addressing uncertainties. Owing to the modeling simplification and various uncertainties, a comprehensive model updating is conducted in this research to correlate numerical simulation with experimental results. The details of this process, together with the system-level parameters, are presented in Section V. Throughout this research, harmonic excitation is provided by a shaker through base excitation, i.e.,

$$F_m = -m_s \cdot a_b \tag{2}$$

where a_b represents the base acceleration, and m_s is the equivalent mass of the base excitation force, the mathematical expression of which can be found in [38], [39], and [40].

The dynamic characteristics of the system are reflected by the transfer function between the mechanical displacement and the external excitation and that between the charge and the external force, i.e.,

$$\frac{\bar{q}}{\bar{F}_m} = \frac{\left(\omega^2 L - i\omega R - k_2\right)}{\left(-m\omega^2 + i\omega g + k\right)\left(\omega^2 L - i\omega R - k_2\right) + k_1^2}$$

$$\frac{\bar{Q}}{\bar{F}_m} = \frac{k_1}{\left(-m\omega^2 + i\omega g + k\right)\left(\omega^2 L - i\omega R - k_2\right) + k_1^2}. \quad (3a, b)$$

Hereafter ω is the excitation frequency and the overbar indicates the magnitude of the corresponding variable.

In this article, we explore the concurrent synthesis of a piezoelectric shunt circuit with inductance and resistance for vibration suppression and energy harvesting. In vibration suppression through resonant shunt, the resistance R can facilitate vibration suppression over a wide frequency range [5], [9]. Meanwhile, in energy harvesting research, it is common practice to apply a resistor load in the piezoelectric circuit and analyze the power of the resistor load to quantify the energy harvesting capability [1], [28], [41]. Power generation of the piezoelectric circuit eventually will be realized by applying various harvesting circuits such as the rectifier circuit [42]. The scope of this article is limited to analyzing the energy harvesting capability, i.e., the power output of resistor load, which is expressed as

$$\bar{P}_s = \bar{V}_s^2 / R \tag{4}$$

where \bar{V}_s is the magnitude of the voltage response crossing the resistor, and can be derived as

$$\frac{\bar{V}_s}{\bar{F}_m} = \frac{i\omega R k_1}{(-m\omega^2 + i\omega g + k)(\omega^2 L - i\omega R - k_2) + k_1^2}.$$
 (5)

We can further derive the ratio between the power output of the resistor load and the square of the excitation magnitude as

$$\left| \frac{\bar{P}_s}{\bar{F}_m^2} \right| = \frac{\omega^2 k_1^2 R}{|A^2 + B^2|} \tag{6}$$

where

$$A = (k - m\omega^2) (\omega^2 L - k_2) + k_1^2 + \omega^2 g R$$

$$B = \omega g (\omega^2 L - k_2) + R\omega (m\omega^2 - k).$$
 (7a,b)

B. Introducing NC

We now take the NC [shown in Fig. 1(b)] into consideration. The NC element that is connected in series with the piezoelectric transducer reduces the reciprocal of piezoelectric capacitance, leading to

$$\hat{k}_2 = k_2 - 1/C_n = 1/C_p - 1/C_n \tag{8}$$

where C_n is the value of the NC. Hereafter the hat notation indicates the system variable with the introduction of the NC circuit.

The introduction of NC changes the response characteristics. For example, the power output of the resistor load is changed to

$$\left| \frac{\dot{\bar{P}}_s}{\bar{F}_m^2} \right| = \frac{\omega^2 k_1^2 R}{\left| \dot{A}^2 + \dot{B}^2 \right|} \tag{9}$$

where \hat{A} and \hat{B} can be obtained by replacing k_2 in (7a) and (7b) with \hat{k}_2 .

C. Tuning for Vibration Suppression and Initial Assessments

As the primary goal of this research is to explore the possibility of enhancing passive vibration using self-sustainable NC, the optimal tuning of the RL elements in the shunt circuit follows the classical derivations [2] that can yield a flat plateau-like frequency response between the mechanical displacement and the external excitation (3a), i.e.,

$$L_{\text{opt}} = \frac{k_2 m}{k}, R_{\text{opt}} = \frac{k_1}{k} \sqrt{2mk_2}$$
 (10a,b)

Similarly, with the introduction of NC, the optimal tuning becomes

$$\hat{L}_{\text{opt}} = \frac{\hat{k}_2 m}{k}, \hat{R}_{\text{opt}} = \frac{k_1}{k} \sqrt{2m\hat{k}_2}.$$
 (11a,b)

The frequency responses between the mechanical displacement and the external excitation of the system with the optimal *RL* shunts under various NC values, together with that without the piezoelectric shunt, are plotted in Fig. 2. As well-known, the *RL* shunt reduces the frequency response peak significantly. The introduction of NC element further reduces the height of the flat plateau-like frequency responses and slightly widens

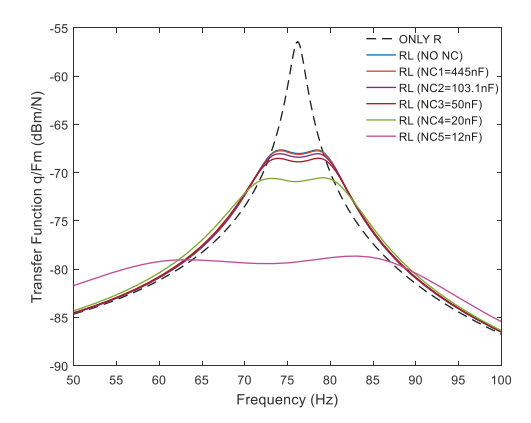


Fig. 2. Optimal vibration suppression performance under different circuits: a passive resistor shunt circuit, a resonant circuit without NC circuit, and resonant circuits with different NC values. Optimal resistance and inductance values are applied in resonant circuits.

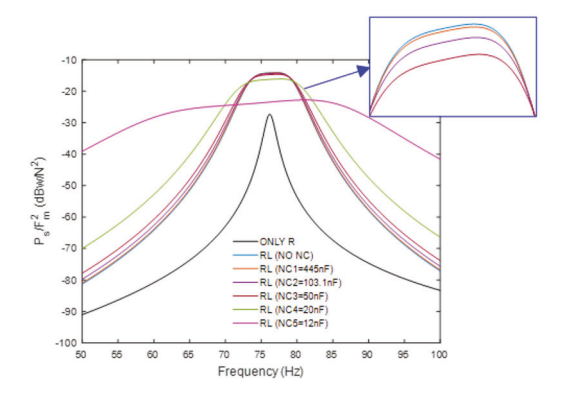


Fig. 3. Available power output under different cases: a passive resistor shunt circuit, a resonant circuit without NC circuit, and resonant circuits with different NC values. In each case, optimal resistance and optimal inductance are applied for optimal vibration suppression performance.

their width. When the NC value (12 nF) approaches the inherent capacitance (11.41 nF) of the particular system analyzed in this research, the frequency response becomes almost completely flat.

The analytical results of the frequency response between the power output of resistor load, i.e., total power available from the energy harvester, and the external excitation are shown in Fig. 3. The first observation is that, with the introduction of the inductance which yields a circuitry resonant frequency which is the same as the mechanical resonant frequency, the available power is significantly increased. When NC element is further introduced, the peak available power actually decreases, while the width of the frequency responses becomes wider. Obviously, there is a complicated tradeoff between vibration reduction and energy harvesting, even before we consider the power consumption of the NC circuit.

III. NC ELEMENT POWER CONSUMPTION

A. Modeling of NC Circuit and Analysis

Here we analyze thoroughly a representative NC circuit shown in Fig. 4. The total voltage of the piezoelectric transducer

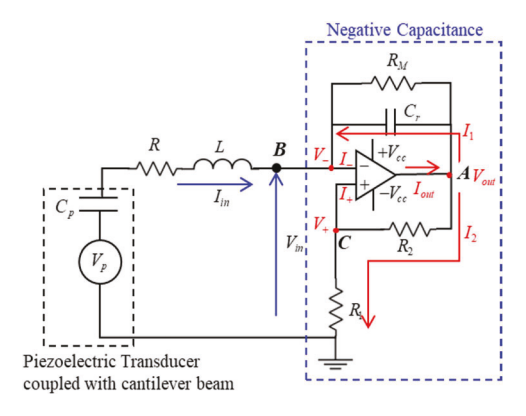


Fig. 4. Detailed equivalent circuit diagram.

is $V_p - k_2 Q$, including the voltage of the inherent capacitance $-k_2 Q$ and the voltage $V_p = -k_1 q$ corresponding to the electromechanical coupling effect which essentially couples the piezoelectric transducer with the mechanical structure. For the series connection studied in this research, the input voltage goes to the inverting pin of the op-amp which is important for realizing the NIC [15], [17]. Assuming the ideal op-amp, we have

$$I_{-} = I_{+} = 0, V_{-} = V_{+} = V_{\text{in}}$$
 (12a,b)

where I_- and I_+ are the currents of the two input pins of the op-amp, and V_- and V_+ are the voltages of points A and B, respectively. $V_{\rm in}$ is the input voltage of the NC circuit which is related to the piezoelectric shunt. The voltage and current of the lower branch involving R_1 and R_2 are

$$V_{\text{out}} = \left(\frac{R_1 + R_2}{R_1}\right) V_+ = \left(\frac{R_1 + R_2}{R_1}\right) V_{\text{in}}$$
 (13)

$$I_2 = \frac{V_{\text{in}}}{R_1} = \frac{V_{\text{out}} - V_{\text{in}}}{R_2} \tag{14}$$

where $V_{\rm out}$ is the output voltage of the op-amp, and I_2 is the lower branch current. In Fig. 4, the upper branch current I_1 represents the total current flowing through the parallel connection of the reference capacitor C_r and a resistor R_M . The resistance value R_M is very large, e.g., chosen as $10.5 {\rm M}\Omega$ in this research. Fundamentally, as discussed in the literature [17], this parallel connection of the reference capacitor C_r and a resistor R_M constitutes a necessary high-pass filter that can solve the implementation issues such as bias-current and offset voltage-induced errors. As such, the current flowing through the resistor is extremely small and can be neglected numerically.

Essentially, the NIC reverses the sign of a reference capacitance C_r . Based on the dependence of the voltages across this reference capacitor, we can derive the following:

$$I_1 = -I_{\rm in} = \frac{V_{\rm out} - V_{\rm in}}{Z_{C_r}} = \frac{R_2}{R_1} i\omega C_r \cdot V_{\rm in}$$
 (15)

$$Z_{\rm in} = \frac{V_{\rm in}}{I_{\rm in}} = \frac{V_{\rm in}}{-I_1} = -\frac{R_1}{R_2} \left(\frac{1}{i\omega C_r}\right)$$
 (16)

where Z_{C_r} is the impedance of the reference capacitor C_r . From (16), we conclude that the impedance of the NC circuit $Z_{\rm in}$ is

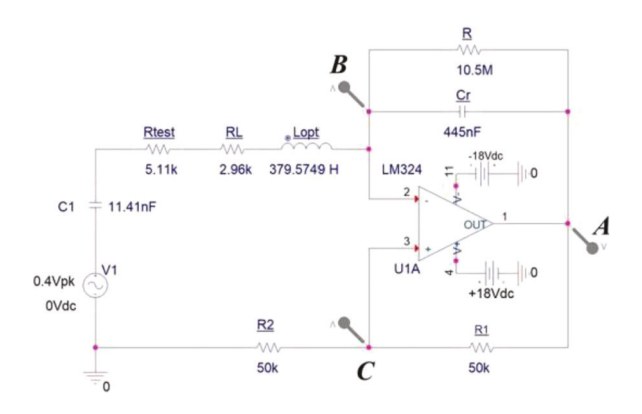


Fig. 5. Circuit simulation model.

equivalent to an NC, i.e.,

$$Z_{\rm in} = -\left(\frac{1}{i\omega C_n}\right). \tag{17}$$

Here

$$-C_n = -\frac{R_2}{R_1}C_r \tag{18}$$

which is the NC achieved.

 I_2 is generally small since resistances R_1 and R_2 are selected to be large in NIC circuit. The value of I_2 is, however, important because in this research we are specifically interested in the power consumption. Based on (13), (14), and (15), we can obtain

$$I_{\text{out}} = I_1 + I_2 = \left(\frac{1 + i\omega C_r R_2}{R_1}\right) \cdot V_{\text{in}}.$$
 (19)

Equations (13) and (19) can lead to power consumption analysis of the NC circuit. Both the output current and output voltage are related to the dynamics of the piezoelectric shunt which is characterized by (1a) and (1b). A preliminary validation of the circuit model can be conducted using PSpice circuit simulation. We consider the combination of piezoelectric shunt [see Fig. 1(b)] and the NC element. The detail of the equivalent circuit is shown in Fig. 4. Since only the circuitry dynamics can be simulated, here the piezoelectric transducer is considered as a voltage source. In practice, such voltage is due to structural vibration through piezoelectric electro-mechanical coupling. In order to match experimental conditions to be analyzed later, the parameters in the simulation are chosen to be the same. The inductor possesses inductance and inherent resistance. We apply the LM324A model of op-amp in simulation, as we will use this op-amp in the subsequent experimental investigation. Three voltage probes, placed at A, B, and C shown in Fig. 5, are employed in the simulation.

The simulation results of the ratio between $I_{\rm in}$ and I_1 and that between $I_{\rm out}$ and I_1+I_2 are shown in Fig. 6. They match well with the analytical results derived in this section. Equation (12) is derived based on ideal op-amp assumption but works well for actual op-amp. For the actual op-amp used, the ratio between V_+ and V_- is slightly different from 1 but the difference is very small within the frequency range of interest.

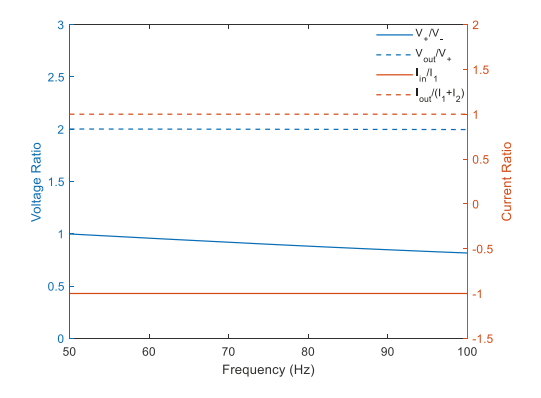


Fig. 6. Circuit simulation results. The ratio V_+/V_- should be equal to1 according to (12b), and the ratio $V_{\rm out}/V_+$ should be equal to 2 according to (13). The analytical value of the current ratio $I_{\rm in}/I_1$ is -1 representing equal and opposite currents, and the analytical value of ratio $I_{\rm out}/(I_1+I_2)$ is 1, which confirms the validity of (19).

B. Power Consumption of NC Circuit

Based on (13) and (19), we now analyze the power consumption of the NC circuit, i.e., the output power of op-amp [20], [21], which can be derived as

$$\bar{\hat{P}}_{\text{op-amp}} = \bar{I}_{\text{out}} \cdot \bar{V}_{\text{out}} = \left(\frac{(R_1 + R_2)(1 + i\omega C_r R_2)}{R_1^2}\right) \cdot \bar{V}_{\text{in}}^2$$
(20)

where \bar{I}_{out} and \bar{V}_{in} are the magnitudes of the input voltage and current of NC circuit, respectively.

The input voltage of the NC circuit can be expressed as

$$\bar{\hat{V}}_{\rm in} = -\bar{\hat{Q}}_{\rm in}/C_n \tag{21}$$

where $\hat{Q}_{\rm in}$, the input charge, is equal to the charged generated by the piezoelectric transducer, \hat{Q} . Recalling (3b), we can obtain the frequency response between NC input voltage and the excitation force as

$$\frac{\bar{\hat{V}}_{\text{in}}}{\bar{F}_m} = \frac{-k_1}{C_n \cdot \left[\left(-m\omega^2 + i\omega g + k \right) \left(\omega^2 L - i\omega R - \hat{k}_2 \right) + k_1^2 \right]}.$$
(22)

The frequency response between the power output of the opamp and the square of the excitation force is then derived as

$$\frac{\bar{\hat{P}}_{\text{op-amp}}}{\bar{F}_{m}^{2}} = \left(\frac{(R_{1} + R_{2})(1 + i\omega C_{r}R_{2})}{R_{1}^{2}C_{n}^{2}}\right) \times \frac{k_{1}^{2}}{\left[(-m\omega^{2} + i\omega g + k)\left(\omega^{2}L - i\omega R - \hat{k}_{2}\right) + k_{1}^{2}\right]^{2}}$$
(23)

which has the following magnitude expression

$$\left| \frac{\bar{P}_{\text{op-amp}}}{\bar{F}_m^2} \right| = \frac{k_1^2 (R_1 + R_2) \sqrt{1 + \omega^2 C_n^2 R_1^2}}{R_1^2 C_n^2 \cdot \left| \hat{A}^2 + \hat{B}^2 \right|}.$$
 (24)

Again, as mentioned previously, \hat{A} and \hat{B} can be obtained by replacing k_2 in (7a) and (7b) with \hat{k}_2 .

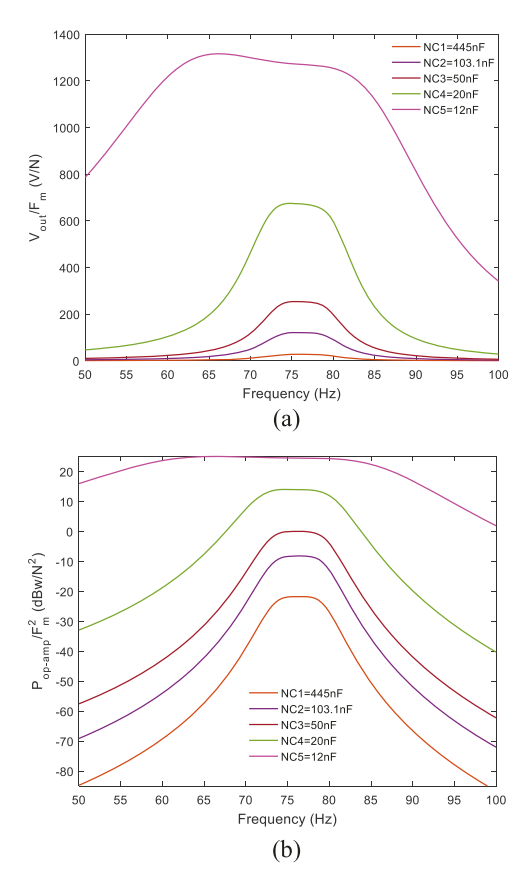


Fig. 7. Frequency responses of (a) output voltage (b) output power of op-amp under different NC values. In each case, optimal resistance and optimal inductance are applied for optimal vibration suppression performance.

In this research, we let $R_1 = R_2 = 50 \text{k}\Omega$ to reduce the number of design variables and attempt to reduce the power consumption of the NC circuit, as larger resistance elements in the NC circuit generally lead to lower power consumption. Fig. 7(a) reports the frequency responses of the output voltage of the op-amp under different NC values. This is not a surprise since the circuitry is coupled with the piezoelectric shunt which itself exhibits a plateau-like frequency response between the mechanical displacement and the external excitation. The output voltage increases dramatically when the NC value gets closer to the inherent piezoelectric capacitance. This indicates that the power output of the op-amp will increase significantly when the NC value approaches the inherent piezoelectric capacitance. Indeed, Fig. 7(b), which plots the frequency response of power consumption, confirms this. The power consumption increase becomes more evident when the NC value gets closer to the inherent piezoelectric capacitance.

IV. System-Level Net Power Analysis

A. Net Power Derivations

The preceding section indicates that a smaller NC value (i.e., closer to the piezoelectric inherent capacitance) leads to the greater power consumption of the NC circuit. Recall Fig. 3

which shows the frequency response of the total power available for harvesting. In that figure, a smaller NC value (i.e., closer to the piezoelectric inherent capacitance) will actually reduce the peak available power. Apparently, a smaller NC value negatively impacts the energy harvesting capability as it reduces the net power of the system which is the difference between the power available for harvesting and the power consumption of the NC circuit. Indeed, the ratio between the net power and the square of external excitation magnitude can be derived as

$$\left| \frac{\dot{\bar{P}}_{\text{net}}}{\bar{F}_{m}^{2}} \right| = \left| \frac{\dot{\bar{P}}_{s}}{\bar{F}_{m}^{2}} \right| - \left| \frac{\dot{\bar{P}}_{\text{op-amp}}}{\bar{F}_{m}^{2}} \right|
= \frac{k_{1}^{2} \left[\omega^{2} R - \frac{(R_{1} + R_{2})}{R_{1}^{2} C_{n}^{2}} \cdot \sqrt{1 + \omega^{2} R_{1}^{2} C_{n}^{2}} \right]}{\left| \hat{A}^{2} + \hat{B}^{2} \right|}.$$
(25)

B. NC Value Selection Criteria for Self-Powering

Equation (25) shows that it is possible to obtain positive net power at the system level, i.e., the difference between the power available for harvesting and the power consumption of the NC circuit. In order to achieve this, the numerator at the right-hand side of (25) must be positive, i.e.,

$$\left[\omega^2 R - \frac{(R_1 + R_2)}{R_1^2 C_n^2} \cdot \sqrt{1 + \omega^2 R_1^2 C_n^2}\right] > 0.$$
 (26)

Recall that we select $R_1 = R_2$ in the NC circuit, and we select R as the optimal value given by (11b) for the purpose of vibration suppression. We can then obtain

$$\frac{k_1}{k}\sqrt{2m\hat{k}_2} > \frac{2}{\omega^2 R_1 C_n^2} \cdot \sqrt{1 + \omega^2 R_1^2 C_n^2}.$$
 (27)

Equation (27) is frequency dependent, representing a condition over a certain frequency range. Since we primarily focus on vibration suppression around the resonant frequency and both the total available power and the power consumption of the NC circuit exhibit plateau-like frequency responses around the resonant frequency, for simplicity we let $\omega = \sqrt{k/m}$. This will allow us to examine the possibility of obtaining positive net power. The parametric tuning for the maximization of positive net power will be subject to future research. As such, we can obtain the following equation for the critical NC value corresponding to zero net power

$$C_n^4 - \frac{1}{k_2}C_n^3 - \frac{2k}{k_2k_1^2}C_n^2 - \frac{2m}{k_2R_1^2k_1^2} = 0.$$
 (28)

Four roots can be solved from the above equation, including two complex conjugate roots, one negative root, and one positive root. Since C_n by definition has to be positive, the positive root corresponds to the critical NC value, above which the system is guaranteed to produce positive net power.

The relation between net power computed from (25) around the resonant frequency and the NC value is plotted in Fig. 8. Apparently, there exists a critical NC value above which the net power is positive. This value matches exactly with the positive root solved from (28), shown as the "*" in the figure. An important finding in this part of the research is that it is indeed

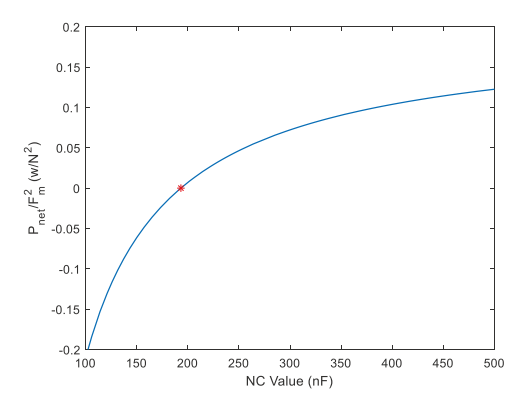


Fig. 8. Net power versus NC value.

possible to achieve positive net power at the system level, which can be used to continuously charge a battery in the integrated system to make the NC circuit self-sustainable.

Equation (28) can only be solved numerically. To acquire further physics insight, we introduce an approximate analysis. Recall (27), we can easily show that

$$\frac{k_1}{k} \sqrt{2m\hat{k}_2} > \frac{2}{\omega^2 R_1 C_n^2} \cdot \sqrt{1 + \omega^2 R_1^2 C_n^2}
> \frac{2}{\omega^2 R_1 C_n^2} \cdot \sqrt{\omega^2 R_1^2 C_n^2} = \frac{2}{\omega C_n}.$$
(29)

We now introduce the definition of the generalized electromechanical coupling coefficient ξ of the original piezoelectric shunt [2]

$$\xi = k_1 / \sqrt{kk_2}.\tag{30}$$

Equation (29) can be rewritten in the nondimensionalized form

$$\frac{C_n}{C_p} > \frac{1 + \sqrt{1 + 8/\xi^2}}{2}. (31)$$

This approximate condition yields the critical NC value 193.26 nF which is fairly close to the accurate value. Interestingly, (31) reveals that the ratio between critical NC value and the inherent capacitance, i.e., the percentage of reduction of the inherent capacitance with positive power being maintained, has to do with the electro-mechanical coupling coefficient of the original shunt. If ξ is larger, the critical NC value can be smaller, implying the capability of better vibration suppression performance enhancement with the NC element while maintaining positive net power.

V. EXPERIMENTAL VALIDATION

A. Experimental Setup and Model Parametric Identification

The setup of the experiment is illustrated in Fig. 9. A cantilever beam (6061 aluminum) is bonded with a piezoelectric transducer (APC 850). An APS 400 shaker connected with an APS 145 power amplifier is used to generate the base excitation. An accelerometer is mounted to the shaker to measure the shaker's

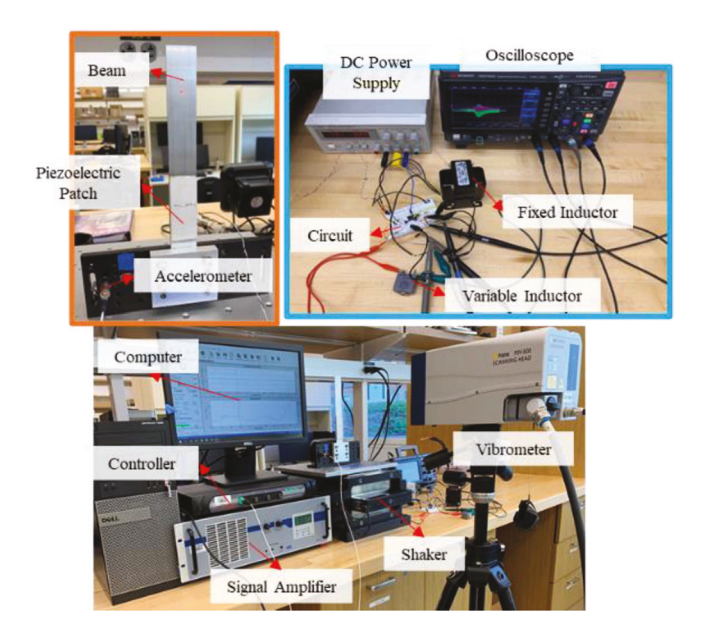


Fig. 9. Experimental setup.

actual acceleration which is fed back to a VR9500P controller to facilitate desired excitation. In this research, we apply frequency sweeping harmonic base excitation with constant acceleration amplitude. The beam response is measured through a Polytec PSV-500 scanning laser vibrometer in a noncontact manner. As mentioned, our primary focus in this research is vibration suppression with NC circuit. The selections of inductance and resistance without NC in the piezoelectric shunt are based on (10a) and (10b), which are 379.57 H and 22.71k Ω . The selection of inductance and resistance with different NC integration are based on (11a) and (11b) by simply replacing k_2 by k_2 . In actual implementation, we employ fixed inductors (Hammond Manufacturing 193A, 193C) connected in series with a variable inductor (HVC-9) to realize the desired optimal inductance value. We use the circuit diagram shown in Fig. 4 to synthesize the NC circuit. The reference capacitance can be conveniently replaced with desired values throughout the experiment. As mentioned, $R_1 = R_2 = 50 \text{ k}\Omega$. R_M is selected as $10.5 \text{M}\Omega$. A dc power supply (Agilent E3630A) is employed to power the opamp. The circuitry frequency responses are measured through a Keysight DSOX1204G digital storage oscilloscope. Both X10 and X100 probes are utilized for voltage measurements. We begin the experimental investigation by examining the system responses without the RL elements in the shunt circuit. The corresponding displacement frequency responses under opencircuit and short-circuit conditions are plotted in Fig. 10, and the open-circuit and short-circuit natural frequencies, $\omega_{\rm open}$ and $\omega_{\rm short}$, are shown in Table III.

There is, inevitably, numerical discrepancy between the simplified model and the actual parameters involved in the analyses, because of the one-mode assumption (1a) and (1b) and the uncertainties in material properties especially those of the piezoelectric transducer. Therefore, as mentioned in Section II, while the classical modeling approach is used as a baseline,

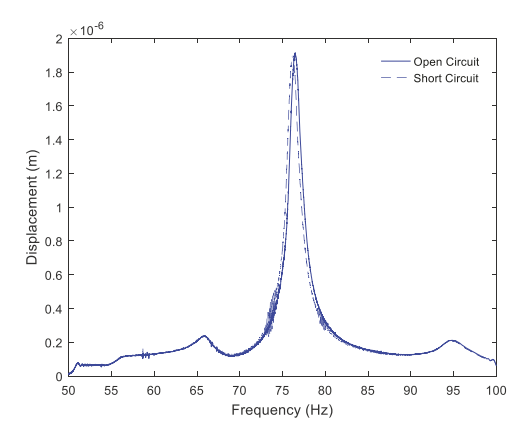


Fig. 10. Experimental results of displacement frequency responses under open-circuit and short-circuit conditions.

TABLE III
EXPERIMENTAL RESULTS

Parameter	Value	Unit
Open circuit Natural frequency	76.4766	Hz
Short circuit Natural frequency	76.1797	Hz
Generalized coupling coefficient	0.0880	-
Optimal resistance without NC	22.707	$\mathrm{k}\Omega$
Optimal inductance without NC	379.5749	Н
Critical NC value	193.26	nF

TABLE IV
MODEL-UPDATED SYSTEM-LEVEL COEFFICIENTS

Parameter	Value	
m	0.0950	
k	2.1942e+04	
g	0.9625	
k_1	1.2210e+05	
k_2	8.7642e+07	
m_s	0.0689	

throughout this research we employ model updating to identify the parameters involved in numerical analyses. This process is summarized as follows. Initially, we collect the measurements of beam mass, piezoelectric transducer mass, and the piezoelectric capacitance. The mass densities are then updated as shown in Tables I and II. Combining the piezoelectric capacitance measurement and the mathematical expression of k_2 [2] which is the reciprocal of the piezoelectric capacitance, we obtain the updated dielectric constant shown in Table II. The Young's moduli of the beam and the piezoelectric transducer follow those provided for the 6061 aluminum and APC 850 transducer, which are listed in Tables I and II. Based on the modeling formulation provided in literature [2] and [38], we can obtain the system-level stiffness k as shown in Table IV.

Our goal is to conduct correlated numerical and experimental investigations to elucidate the power consumption of op-amp-based NC circuit. Hence, here we identify, directly, the system-level mass m from the open-circuit natural frequency $\omega_{\mathrm{open}} = \sqrt{k/m}$. Subsequently, the electro-mechanical coupling constant k_1 can be identified from the short-circuit natural frequency $\omega_{\mathrm{short}} = \sqrt{(k-k_1^2/k_2)/m}$. They are shown in Table IV. Since k_1 is dependent upon the piezoelectric constant of the transducer, using literature modeling formulation [2] we further update the piezoelectric constant as shown in Table II. The damping coefficient g listed in Table IV is identified through the three-dB method. Finally, the equivalent mass of base excitation force is identified by matching the experimental displacement frequency response peaks with the numerical simulation results, which are listed in Table IV.

The electro-mechanical coupling coefficient can be calculated as

$$\xi = \sqrt{\frac{\omega_{\text{open}}^2 - \omega_{\text{short}}^2}{\omega_{\text{open}}^2}}.$$
 (32)

Subsequently, the optimal inductance and resistance values employed in the experiment can be obtained based on experimental results as follows:

$$L_{\text{opt}} = \frac{1}{C_p \cdot \omega_{\text{open}}^2}, R_{\text{opt}} = \frac{\sqrt{2}\xi}{C_p \cdot \omega_{\text{open}}^2}$$
(33a,b)

which are provided in Table III. For this particular experimental setup, the optimal inductance value is large. One way of resolving this issue is to replace the passive inductors with synthetic inductance circuit based on op-amp circuit. The synthetic inductance requires power supply as well. Since this research focuses on whether it is possible to have positive net power when the NC circuit is incorporated, we only use passive inductors in the experiment.

B. Optimal Vibration Suppression

It is well known that piezoelectric shunt with *RL* elements can effectively suppress vibration. Here we present some experimental results to illustrate the enhancement by means of NC circuit integration. This will provide insight into the tradeoff between vibration suppression enhancement and the net power for energy harvesting.

The beam velocity frequency response measurements are shown in Fig. 11. Without the piezoelectric shunt, the original beam has excessive vibration. The integration of the piezoelectric shunt with optimal RL selections can greatly reduce the vibration. When we introduce an NC circuit with NC 445 nF into the piezoelectric shunt, the beam vibration can be reduced further by approximately 14.39% at short-circuit resonant frequency. This is a significant enhancement in vibration suppression. According to the analytical results presented in Section II-B, as far as vibration suppression is concerned, we can introduce NC values that are closer to the piezoelectric inherent capacitance. Recall that the inherent capacitance of the piezoelectric transducer is 11.41 nF. Indeed, when we introduce an NC 103.1 nF, we can observe additional vibration suppression (20.89%) with respect to that under NC 445 nF (14.39%). Nevertheless, the additional performance gain in this second NC circuit case appears to be limited even with a quite large

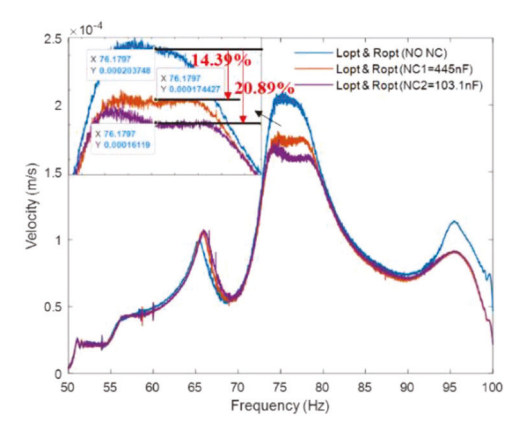


Fig. 11 Experimental frequency responses of vibration velocity magnitude. Three different cases are considered: resonant circuit with ut NC; resonant circuit with 445 nF NC; resonant circuit with 103.1 nF NC.

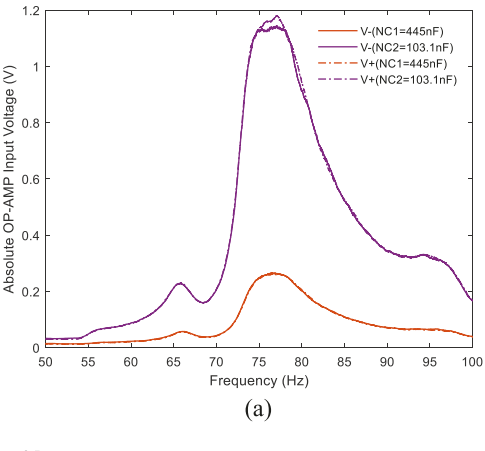
difference in NC values. This is consistent with the analytical prediction presented in Section II-C.

C. Self-Powering Capability Validation

The goal of this research is to explore a self-sustainable vibration suppression enhancement scheme with NC element and energy harvesting. Here we systematically investigate, through experiment, the NC circuit characteristics as well as the output power of the resistor load (i.e., the power available for energy harvesting), the power consumption of the NC element, and most importantly the net power at the system level.

The analysis of power consumption of the NC circuit is built upon the voltage relationships expressed in (12b) and (13). In Section III-A, we have conducted a preliminary validation of the NC circuit model, where the piezoelectric transducer is modeled as an equivalent voltage source but its coupling with the mechanical structure is not included. As such, while the various ratios of voltages and currents, e.g., $V_+/V_- = 1$, $V_{\text{out}}/V_{\text{in}} = 2$, $I_{\rm in}/I_1=-1$, and $I_{\rm out}/(I_1+I_2)=1$, have been confirmed, the respective voltages and currents do not exhibit the effect of mechanical resonance. Here as a thorough examination, we measure directly the two input voltages and the output voltage of the op-amp whereas the piezoelectric shunt is fully coupled with the mechanical structure in the experiment. As can be observed in Fig. 12, all the related voltage responses exhibit peaks at the beam natural frequency 76.48 Hz, and the peaks exhibit correspondingly plateau-like patterns owing to the optimal tuning of the RL elements in the shunt for vibration suppression. Moreover, even with the resonant behaviors, the related voltage ratios agree with the analytical results, i.e., $V_{+}/V_{-}=1$, and $V_{\rm out}/V_{\rm in}=2$, for both NC values, i.e., 103.1 and 445 nF. In the circuit simulation results shown in Fig. 6, the piezoelectric coupling is not included. The experimental results reported in Fig. 12 further indicate that the op-amp analysis outlined in Section III-A is valid when the piezoelectric shunt circuit is integrated together.

We now analyze the NC circuit power consumption. In Section III, we have derived the analytical results of its output



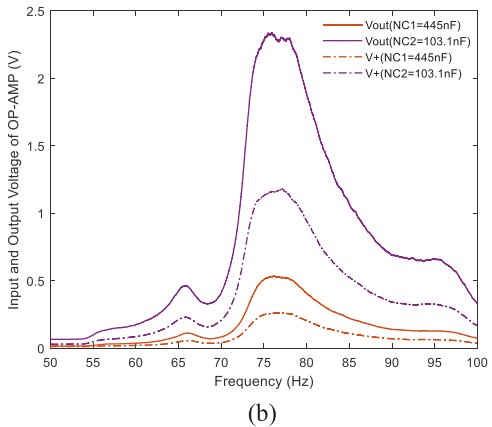


Fig. 12. Voltage relationships in NC circuit under different NC values.
(a) Voltage frequency responses of two input terminals of the op-amp.
(b) Correlation between op-amp output voltage and input voltage.

voltage in (13), output current in (19), and power consumption in (20). The analytical and experimental results of output voltage of op-amp and power consumption of NC circuit are reported in Fig. 13. As can be observed in Fig. 13(a), for both NC values, the experimental results of output voltage match very well with the analytical results. Fig. 13(b) shows the power consumption of the NC circuit. When the NC value is 445 nF, the analytical and experimental results match very well. When the NC value is 103.1 nF, the two results still match approximately. While there exists an error, the error generally is due to the small amplitude of the current value measured in the experiment. The error is more noticeable when the NC value is closer to the piezoelectric inherent capacitance, since the response becomes more sensitive to various uncertainties of the circuitry elements involved in such a situation. Nevertheless, the analytical and experimental results match reasonably well. It should be noted that the smaller NC value, 103.1 nF, results in a remarkable increase (almost 500%) in output voltage. Consequently, the power consumption also significantly increased. These comparisons demonstrate the validity of the op-amp power analysis. Future investigations may focus on how to improve the circuitry performance through employing different circuitry parametric tunings or even different NC circuit configurations when the NC value is closer to the piezoelectric inherent capacitance.

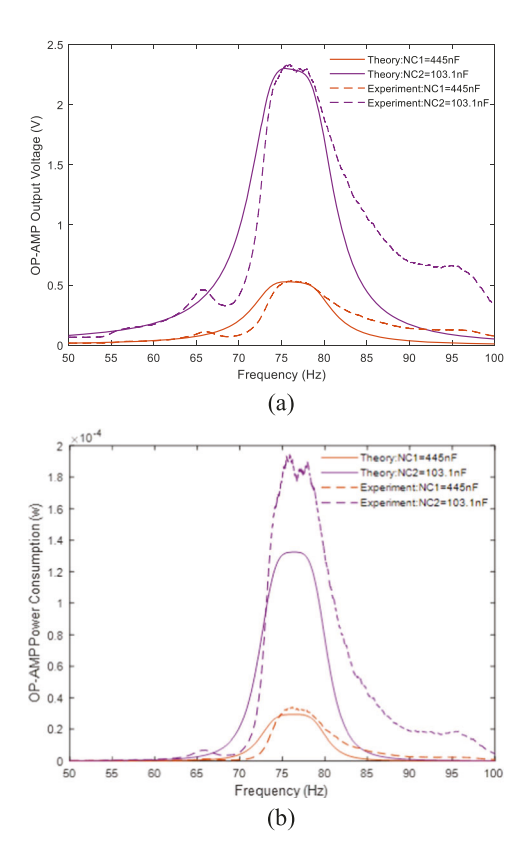


Fig. 13. Frequency responses of (a) op-amp output voltage and (b) power consumption of NC circuit under different NC values. Both analytical results and experiments are displayed in each plot.

We then analyze the available power for energy harvesting, i.e., the power of the resistor load R in the piezoelectric circuit in (6). Both the analytical and experimental results are plotted in Fig. 14, which show good agreement. It is worth noting that our goal is to enhance vibration suppression. As we tune the NC value, the optimal R value is also adjusted correspondingly to realize optimal vibration suppression. Consequently, the available power of the resistor load does not see a significant increase even though the generalized electro-mechanical coupling is increased by the introduction of the NC circuit.

The preceding experimental results demonstrate the validity of the analyses on available power and power consumption of NC circuit. Finally, we examine experimentally the net power at the system level, which is the difference between the available power and the power consumption of the NC circuit in (25). The experimental results of net power under the two representative NC values, 445 nF (above the critical NC value) and 103.1 nF (below the critical NC value) that are analyzed in this research, are shown in Fig. 15. Fig. 15 reports an important confirmation that, when the NC value is selected to be above the critical value (derived in Section IV-B), we can achieve positive net power. This leads to the finding that a self-sustainable vibration suppression enhancement with an NC circuit is feasible. As the net power is positive, the energy harvesting component of the integrated circuitry system can constantly charge a rechargeable battery to sustain the operation of the NC circuit. When the NC

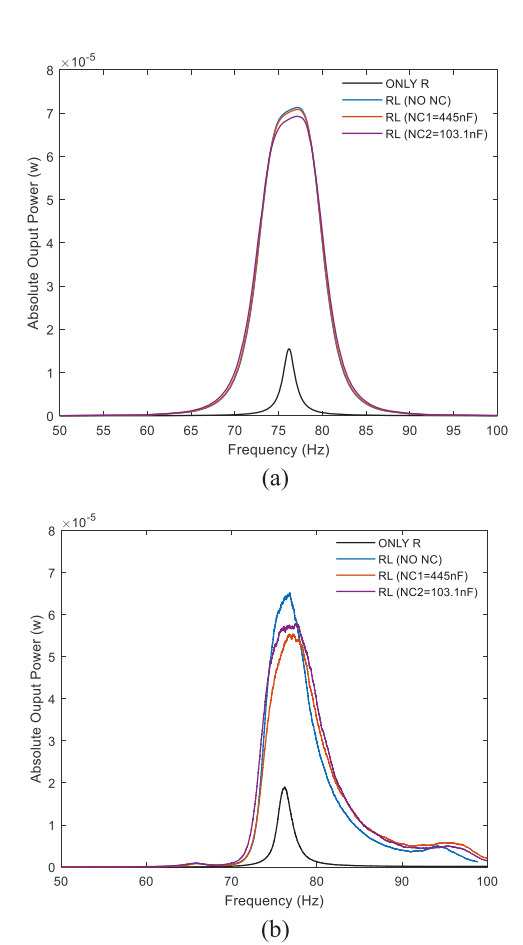


Fig. 14. Frequency responses of available power of load resistor. (a) Analytical results. (b) Experimental results. Four different cases are considered: resistive circuit; resonant circuit without NC; resonant circuit with 445 nF NC; resonant circuit with 103.1 nF NC.

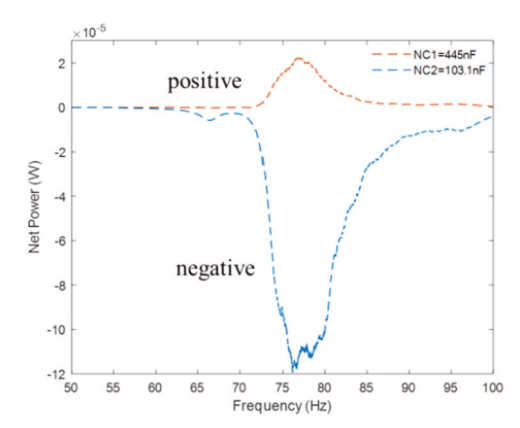


Fig. 15. Experimental frequency responses of net power under different NC values.

value is selected as 103.1 nF which is below the critical value, the net power becomes negative, as shown in Fig. 15. These results indicate that there indeed exists a range of NC values that can yield positive net power for this integration. The optimization of such a self-sustainable enhanced system can be subject to future research, based on practical performance metrics.

VI. CONCLUSION

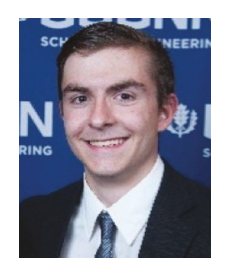
This article explores the feasibility of synthesizing a selfsustainable vibration suppression enhancement scheme utilizing piezoelectric shunt with NC element where the energy harvesting capability of the piezoelectric transducer is exploited. Systematic analysis of NC circuit is conducted to analyze its power consumption when it is integrated into the piezoelectric shunt. We then investigate the parametric influence of the NC element on vibration suppression and the net power, i.e., the difference between available power for energy harvesting and the op-amp power consumption. It is analytically identified and experimentally confirmed that a self-sustainable vibration enhancement scheme is realizable. For example, for one NC value 445 nF selected, the system will yield 14.39% more vibration reduction at short-circuit resonant frequency while achieving positive net power. The analysis methodology can be applied to parametric optimization as well as other piezoelectric systems integrated with NC element.

REFERENCES

- [1] T. S. Todorov, A. S. Fursov, R. P. Mitrev, V. V. Fomichev, S. S. Valtchev, and A. V. II'in, "Energy harvesting with thermally induced vibrations in shape memory alloys by a constant temperature heater," *IEEE/ASME Trans. Mechatron.*, vol. 27, no. 1, pp. 475–484, Feb. 2022.
- [2] J. Tang and K. W. Wang, "Active-passive hybrid piezoelectric networks for vibration control: Comparisons and improvement," *Smart Mater. Struct.*, vol. 10, no. 4, pp. 794–806, Aug. 2001.
- [3] K. W. Wang and J. Tang, Adaptive Structural Systems With Piezoelectric Transducer Circuitry. Berlin, Germany: Springer-Verlag, 2009.
- [4] K. Marakakis, G. K. Tairidis, P. Koutsianitis, and G. E. Stavroulakis, "Shunt piezoelectric systems for noise and vibration control: A review," Front. Built Environ., vol. 5, pp. 64–80, May. 2019.
- [5] N. W. Hagood and A. V. Flotow, "Damping of structural vibrations with piezoelectric materials and passive electrical networks," *J. Sound Vib.*, vol. 146, no. 2, pp. 243–268, Apr. 1991.
- [6] L. Zuo and S. A. Nayfeh, "Optimization of the individual stiffness and damping parameters in multiple-tuned-mass-damper systems," *J. Vib. Acoust.*, vol. 127, no. 1, pp. 77–83, Feb. 2005.
- [7] Y. Luo, H. Sun, X. Wang, A. Chen, and L. Zuoturn, "Parametric optimization of electromagnetic tuned inerter damper for structural vibration suppression," *Struct. Control Health Monit.*, vol. 28, no. 5, May 2021, Art. no. e2711.
- [8] F. Zhang, J. Liu, and J. Tian, "Analysis of the vibration suppression of double-beam system via nonlinear switching piezoelectric network," *Machines*, vol. 9, no. 6, pp. 115–135, Jun. 2021.
- [9] P. Gardonio, M. Zientek, and L. Dal Bo, "Panel with self-tuning shunted piezoelectric patches for broadband flexural vibration control," *Mech. Syst. Signal Process*, vol. 134, pp. 106299–106321, Dec. 2019.
- [10] J. F. Toftekær and J. Høgsberg, "Multi-mode piezoelectric shunt damping with residual mode correction by evaluation of modal charge and voltage," *J. Intell. Mater. Syst. Struct.*, vol. 31, no. 4, pp. 570–586, Mar. 2020.
- [11] Y. Wu, X. Liu, A. Badel, H. Ji, and J. Qiu, "Semi-active piezoelectric structural damping adjustment and enhancement by synchronized switching on energy injection technique," *J. Sound Vib.*, vol. 527, Feb. 2022, Art. no. 116866.
- [12] M. Chen et al., "Design and analysis of piezoelectric micromachined ultrasonic transducer using high coupling PMN-PT single crystal thin film for ultrasound imaging," Smart Mater. Struct., vol. 30, no. 5, Mar. 2021, Art. no. 055006.
- [13] S. A. Mansoura, P. Bénard, B. Morvan, P. Maréchal, A. C. Hladky-Hennion, and B. Dubus, "Theoretical and experimental analysis of a piezoelectric plate connected to a negative capacitance at MHz frequencies," *Smart Mater. Struct.*, vol. 24, pp. 115032–115038, Oct. 2015.
- [14] B. Götz, M. Schaeffner, R. Platz, and T. Melz, "Lateral vibration attenuation of a beam with circular cross-section by a support with integrated piezoelectric transducers shunted to negative capacitances," *Smart Mater. Struct.*, vol. 25, no. 9, pp. 095045–095054, Aug. 2016.

- [15] T. M. P. Silva, M. A. Clementino, V. C. de Sousa, and C. De Marqui, "An experimental study of a piezoelectric metastructure with adaptive resonant shunt circuits," *IEEE/ASME Trans. Mechatron.*, vol. 25, no. 2, pp. 1076–1083, Apr. 2020.
- [16] J. A. B. Gripp, L. C. Goes, O. Heuss, and F. Scinocca, "An adaptive piezoelectric vibration absorber enhanced by a negative capacitance applied to a shell structure," *Smart Mater. Struct.*, vol. 24, no. 12, pp. 125017–125031, Nov. 2015.
- [17] M. Berardengo, O. Thomas, C. Giraud-Audine, and S. Manzoni, "Improved resistive shunt by means of negative capacitance: New circuit, performances and multi-mode control," *Smart Mater. Struct.*, vol. 25, no. 7, pp. 075033–075055, Jun. 2016.
- [18] K. Billon et al., "Vibration isolation and damping using a piezoelectric flextensional suspension with a negative capacitance shunt," *Mech. Syst. Signal Process*, vol. 140, pp. 106696–106706, Jun. 2020.
- [19] M. Berardengo, S. Manzoni, M. Vanali, and R. Bonsignori, "Enhancement of the broadband vibration attenuation of a resistive piezoelectric shunt," *J. Intell. Mater. Syst. Struct.*, vol. 32, no. 18/19, pp. 2174–2189, Nov. 2021, doi: 10.1177/1045389X20988090.
- [20] B. S. Beck, K. A. Cunefare, and M. Collet, "The power output and efficiency of a negative capacitance shunt for vibration control of a flexural system," *Smart Mater. Struct.*, vol. 22, no. 6, pp. 065009–065018, Apr. 2013.
- [21] E. M. Qureshi, X. Shen, and L. Chang, "Power output and efficiency of a negative capacitance and inductance shunt for structural vibration control under broadband excitation," *Int. J. Aeronaut.*, vol. 16, no. 2, pp. 223–246, Jun. 2015.
- [22] Y. Wang and D. J. Inman, "A survey of control strategies for simultaneous vibration suppression and energy harvesting via piezoceramics," *J. Intell. Mater. Syst. Struct.*, vol. 23, no. 18, pp. 2021–2037, Dec. 2012.
- [23] S. Li, J. Xu, and J. Tang, "Tunable modulation of refracted lamb wave front facilitated by adaptive elastic metasurfaces," *Appl. Phys. Lett.*, vol. 112, no. 2, Jan. 2018, Art. no. 021903.
- [24] C. Sugino, M. Ruzzene, and A. Erturk, "Design and analysis of piezoelectric metamaterial beams with synthetic impedance shunt circuits," *IEEE/ASME Trans. Mechatron.*, vol. 23, no. 5, pp. 2144–2155, Oct. 2018.
- [25] G. Hu, L. Tang, J. Xu, C. Lan, and R. Das, "Metamaterial with local resonators coupled by negative stiffness springs for enhanced vibration suppression," J. Appl. Mech., vol. 86, no. 8, Aug. 2019, Art. no. 081009.
- [26] G. Hu, J. Xu, L. Tang, C. Lan, and R. Das, "Tunable metamaterial beam using negative capacitor for local resonators coupling," *J. Intell. Mater.* Syst. Struct., vol. 31, no. 3, pp. 389–407, Feb. 2020.
- [27] Z. Yaw, W. Zhou, and C. W. Lim, "Anomalous wave control by an adaptive elastic metasurface shunted with negative capacitance circuit," *J. Sound Vib.*, vol. 525, May. 2022, Art. no. 116782.
- [28] A. González, J. L. Olazagoitia, J. Viñolas, I. Ulacia, and M. Izquierdo, "An innovative energy harvesting shock absorber system for motorbikes," *IEEE/ASME Trans. Mechatron.*, vol. 27, no. 5, pp. 3110–3120, Oct. 2022.
- [29] H. X. Zou et al., "Mechanical modulations for enhancing energy harvesting: Principles, methods and applications," *Appl. Energy*, vol. 255, Dec. 2019, Art. no. 113871.
- [30] M. Cai, Z. Yang, J. Cao, and W. H. Liao, "Recent advances in human motion excited energy harvesting systems for wearables," *Energy Technol.*, vol. 8, no. 10, Oct. 2020, Art. no. 2000533.
- [31] F. Gao, G. Liu, X. Fu, L. Li, and W.-H. Liao, "Lightweight piezoelectric bending beam-based energy harvester for capturing energy from human knee motion," *IEEE/ASME Trans. Mechatron.*, vol. 27, no. 3, pp. 1256–1266, Jun. 2022.
- [32] G. Shi et al., "A sensorless self-tuning resonance system for piezoelectric broadband vibration energy harvesting," *IEEE Trans. Ind. Electron.*, vol. 68, no. 3, pp. 2225–2235, Mar. 2021.
- [33] N. Chen, T. Wei, D. S. Ha, H. J. Jung, and S. Lee, "Alternating resistive impedance matching for an impact-type microwind piezoelectric energy harvester," *IEEE Trans. Ind. Electron.*, vol. 65, no. 9, pp. 7374–7382, Sep. 2018.
- [34] L. Liu, Y. Xing, W. Huang, X. Liao, and Y. Li, "A 10 mV-500 mV input range, 91.4% peak efficiency adaptive multi-mode boost converter for thermoelectric energy harvesting," *IEEE Trans. Circuits Syst. I Reg. Paper*, vol. 69, no. 2, pp. 609–619, Feb. 2022.
- [35] F. Qian, M. R. Hajj, and L. Zuo, "Bio-inspired bi-stable piezoelectric harvester for broadband vibration energy harvesting," *Energy Convers. Manage.*, vol. 222, Oct. 2020, Art. no. 113174.
- [36] Y. Gao, J. Liang, and Y. Liao, "Multiple harmonics extended impedance model of piezoelectric energy harvesting systems," *IEEE/ASME Trans. Mechatron.*, vol. 27, no. 2, pp. 1185–1195, Apr. 2022.

- [37] N. M. Monroe and J. H. Lang, "Broadband, large scale acoustic energy harvesting via synthesized electrical load: II. Electrical load," *Smart Mater. Struct.*, vol. 28, no. 5, Apr. 2019, Art. no. 055033.
- [38] C. Lan, Y. Liao, G. Hu, and L. Tang, "Equivalent impedance and power analysis of monostable piezoelectric energy harvesters," *J. Intell. Mater.* Syst. Struct., vol. 31, no. 14, pp. 1697–1715, Aug. 2020.
- [39] W. Zhou and L. Zuo, "A self-powered piezoelectric vibration control system with switch precharged inductor (SPCI) method," *IEEE/ASME Trans. Mechatron.*, vol. 20, no. 2, pp. 773–781, Apr. 2015.
- [40] Y. Liao and H. A. Sodano, "Model of a single mode energy harvester and properties for optimal power generation," *Smart Mater. Struct.*, vol. 17, no. 6, Nov. 2008, Art. no. 065026.
- [41] J. Wang and L. Zhao, "Toward nonlinear galloping energy harvesting interfaced with different power extraction circuits," *IEEE/ASME Trans. Mechatron.*, vol. 27, no. 5, pp. 2678–2689, Oct. 2022.
- [42] M. Edla, Y. Y. Lim, M. Deguchi, R. V. Padilla, and I. Izadgoshasb, "An improved self-powered H-bridge circuit for voltage rectification of piezoelectric energy harvesting system," *IEEE. J. Electron Devices Soc.*, vol. 8, pp. 1050–1062, 2020.



energy harvesting.

Joshua Dupont (Student Member, IEEE) received the B.S. degrees in mechanical engineering and electrical engineering, in 2020, from the University of Connecticut, Storrs, CT, USA, where he is currently working toward the Ph.D. degree in mechatronic synthesis for vibration suppression and acoustic wave manipulation with the Department of Mechanical Engineering.

His research interests include elastic metamaterials, waveguiding, vibration isolation, and



Ting Wang (Graduate Student Member, IEEE) received the B.S. degree in logistics engineering and the M.S. degree in mechatronics engineering from the School of Mechanical Engineering, Dalian University of Technology, Dalian, China, in 2016 and 2019, respectively. She is currently working toward the Ph.D. degree in mechatronic synthesis for energy harvesting and metamaterial design with the Department of Mechanical Engineering, University of Connecticut, Storrs, CT, USA.

She is a Research Assistant with the Department of Mechanical Engineering, University of Connecticut. Her research interests include smart materials, energy harvesting, vibration suppression, and metamaterials.



Jiong Tang (Member, IEEE) received the B.S. and M.S. degrees in applied mechanics from the Fudan University, Shanghai, China, in 1989 and 1992, respectively, and the Ph.D. degree in mechanical engineering from the Pennsylvania State University, State College, PA, USA, in 2001.

He is the Pratt & Whitney Professor of Advanced Materials and Processing with the Department of Mechanical Engineering, University of Connecticut, Storrs, CT, USA. His re-

search interests include dynamics, sensing, control, and automation. Dr. Tang is a fellow of the ASME.